JOURNAL OF MATERIALS SCIENCE 33 (1998) 2607–2616

Niobia films: surface morphology, surface analysis, photoelectrochemical properties and crystallization process

D. de A. B. FILHO, D. W. FRANCO
Instituto de Química de São Carlos, Av. Dr. Carlos Botelho, 1465, Caixa Postal 780, 13560-970 São Carlos SP, Brazil
E-mail: dougas@iqsc.sc.usp.br.

P. P. A. FILHO, O. L. ALVES
Instituto de Química, Universidade Estadual de Campinas, UNICAMP, CP 6154, 13083-970 Campinas SP, Brazil

The photoelectrochemical properties of sol–gel Nb_2O_5 coatings have been discussed in terms of their surface morphology. Niobium chloroalkoxide solution was prepared and thin films were deposited by dip-coating on the indium–tin oxide conductor glass. Structural, optical and electro-properties of amorphous and crystalline sol–gel coatings have been determined. Powders were prepared by the hydrolysis of amorphous niobium and were characterized by X-ray diffraction and electron paramagnetic resonance. These measurements indicated which changes were introduced in the photoelectrical behaviour of the semiconductor due to its crystalline structure. The absorption measurements showed an absorption band in the ultraviolet range associated with the electronic transfer $O^{2-} \rightarrow Nb^{5+}$ whose energy gap was around 3.3 eV. The photoelectrochemical measurements for the coatings were done in lithium perclorate and were used to determine the flat band potential, V_{bp}, and the electron diffusion length, L. The influence of particle sizes in the charge-transfer process at the semiconductor–electrolyte interface was discussed according to the models of Gärtner and Södergren. © *1998 Chapman & Hall*

1. Introduction

Films made of semiconductor particles with nanoporous morphology and high surface area are currently of great interest, particularly after the dye-sensitized solar cell reported by Grätzel [1–3]. This solar cell is based on a thin nanocrystalline TiO_2 film with particle diameters of typically 15–20 nm, which are dye-sensitized by a ruthenium–bipyridyl complex.

An important aspect of a semiconductor is the analysis of the charge-transfer process in the semiconductor–electrolyte interface (SEI) which involves chemical–physical aspects, such as chemical reactions, surface states [4], optical absorption, etc. The chemical reactions occurring in the electrolyte are an important part [5] because of the ionic transport that results in the conversion of light energy into electrical energy.

In this paper, we report the preparation of semiconducting Nb_2O_5 films and the characterization of their structural, optical and photoelectrochemical properties. These films may be an alternative for the development of solar to electrical energy conversion devices.

2. Experimental procedure

Niobia films were prepared by dipping a conducting glass support (indium–tin oxide (ITO)-coated glass with a resistance of 14 Ω/□, Donelly Corporation) in a solution of niobium chloroalkoxide in *n*-butyl alcohol and pulling it up at 12 cm h^{-1}.

The niobium chloroalkoxide was prepared by the method first described by Bradley *et al.* [6]. In this work, 11.5 g $NbCl_5$ (CBMM, Brazil) was dissolved in 40 ml dry *n*-butyl alcohol (Aldrich) to which was added 250 ml dry cyclohexane (Merck). Afterwards, dry NH_3 was bubbled through to remove the Cl-ions by precipitation of ammonium chloride. This precipitate was removed by filtration and the solvents evaporated by distillation under an argon atmosphere. All the reactions and manipulations in this procedure were carried out using standard Schlenk techniques.

The niobium content was determined by gravimetry where it was precipitated as the hydroxide, washed with hot water and ignited to Nb_2O_5. The chlorine was determined in the wash liquid from the niobium determination by volumetric analysis using the Mohr method [7]. The results of these chemical determinations gave the following minimum formula for niobium chloroalkoxide: $NbCl(OBut)_4$. The yield obtained in this procedure was 63%.

The solutions, used in the deposition of the films, were prepared by dilution of niobium chloroalkoxide in *n*-butyl alcohol in the concentration range of

1%–8% (mol/mol). The technique of dip-coating consisted in dipping the ITO glass, which had previously been cleaned, in the niobium chloroalkoxide solutions. After this, the coating was dried under room conditions and then heated up to 350 °C and held at this temperature for 5 min. The whole process was repeated in order to increase the thickness of the films. The final films were heated under air at the desired temperature (400 °C $< T <$ 600 °C) for 2 h. The thickness of the films, d, was measured using a Taylor Hobson Talystep.

The ultraviolet absorption spectra of the films were obtained using a Cary 17 spectrophotometer from films deposited on quartz plates using the same procedure described for the ITO substrate. The electron-probe microanalysis of the films was done using an energy dispersive spectrometer (EDS), Zeiss model DSM 960. The morphologies of the films were analysed by using a scanning electron microscope (SEM). In the EDS and SEM analysis, the film and substrate were just glued with conductive paint to the holder and gold coated.

The photoelectrochemical response of the films was determined using an electrochemical cell built with Teflon and having a quartz window for light excitation from a calibrated Bausch and Lomb system comprising a 150 W xenon lamp coupled to a high-intensity monochromator (bandwidth 16 nm). The monochromatic light output, I_{hv}, was quantitatively calibrated using a Labmaster/Fieldmaster coherent LM2 and LM-2UV detector down to 250 nm. The action spectra were measured in reference to a saturated calomel electrode (SCE) and a platinum foil as counter electrode. The electrolytes used were an aqueous solution of $LiClO_4$ 0.2 mol l^{-1} and a solution of $LiClO_4$ 1 mol l^{-1} in propylene carbonate (Aldrich). The volume of the electrolyte inside the cell was 50 ml and when aqueous solutions were used it was saturated with dry nitrogen gas to avoid surface states. The circular area of the light irradiation was kept to 1 cm diameter, and the optical path to 6.5 cm. The measurements were performed using a computerized PAR model 273-A potentiostat.

The niobia powders were prepared by hydrolysis of niobium chloroalkoxide solutions with hot H_2O, resulting in the precipitation of niobium as hydroxide. This hydroxide was collected by filtration and washed with hot H_2O to eliminate the Cl^- ions. Afterwards, the solid was dried at 120 °C, resulting in the sample identified as the initial sample before heat treatment. Later, the solids were heated in an oven at the desired temperature (400 °C $< T <$ 1200 °C) for 2 h in air.

X-ray diffractograms were obtained at room temperature using a Schimadzu (XD-3A) diffractometer with CuK_α radiation generated at 35 kV and 25 mA.

Electron paramagnetic resonance (EPR) spectra were taken in a computerized spectrometer, Bruker model ESP-300e, operating at 9.44 GHz (X-band) and the microwave power was 20 mW. The spectra were obtained at liquid nitrogen temperature with irradiation of the samples by a 150 W xenon lamp.

3. Experimental results

3.1. Thermal transformations

The niobia powder undergoes thermal transformations when heated at temperatures smaller than 1000 °C. The material is amorphous until 400 °C (Fig. 1a and b). In the 500–600 °C range, it shows diffraction peaks assigned to the δ-phase (Fig. 1c and d). At 800 °C, new diffraction peaks are observed (Fig. 1e), but these do not agree with those observed in the 500–600 °C range. In this range, another crystalline phase, identified as γ-phase emerges. On further heating to 1000 °C, the solid undergoes another transformation, resulting in an α-phase (Fig. 1f). All the crystalline phases were identified by comparison with the literature data [8].

3.2. EPR measurements for niobium pentoxide powders

Fig. 2 shows the EPR measurements of the powder after light irradiation. There are two resident signals associated with the generation of an unpaired electron in the semiconductor structure. The first signal with $g = 2.0$ is a hole centre generated by the oxygen present in the semiconductor [9]. The second signal with

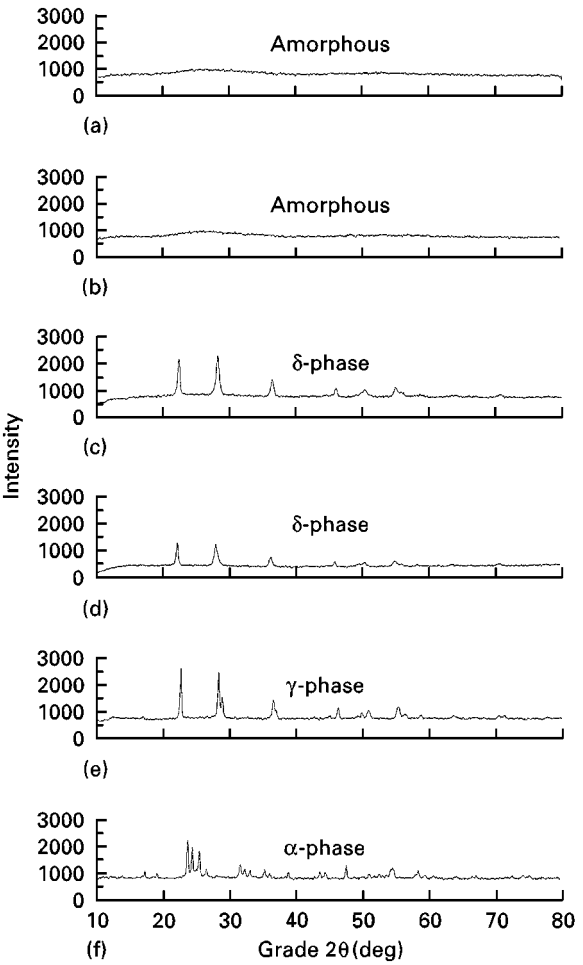

Figure 1 X-ray measurements for niobium oxide powders treated at different heat-treatment temperatures, T: (a) initial sample; (b) 400 °C; (c) 500 °C; (d) 600 °C; (e) 800 °C; (f) 1000 °C. θ is the X-ray incidence angle.

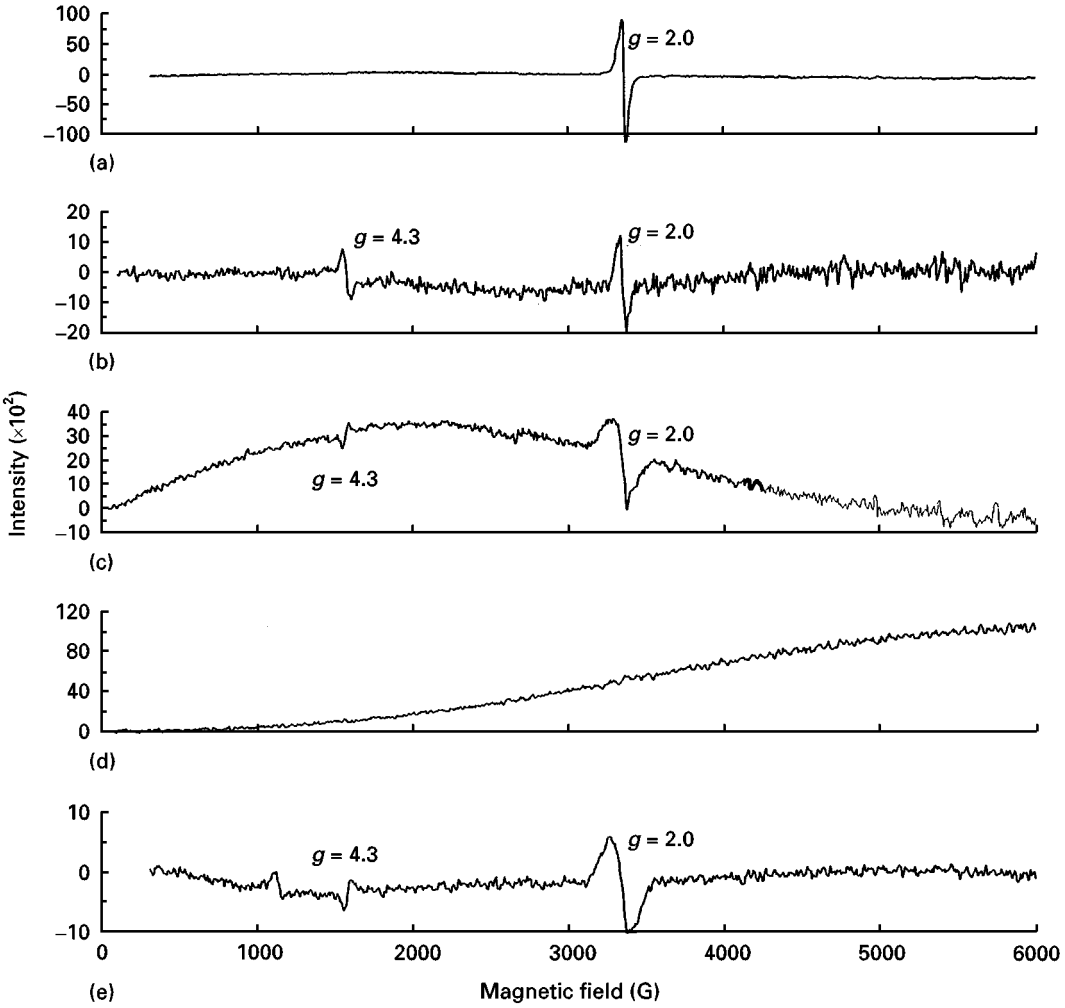

Figure 2 Electron paramagnetic resonance (EPR) measurements for niobium oxide powders treated at different heat-treatment temperatures: (a) initial sample; (b) 400 °C; (c) 500 °C; (d) 600 °C; (e) 800 °C. ($g = 2.0$) is the hole defect centre associated with an oxygen atom; ($g = 4.3$) is the iron impurity.

$g = 4.3$ is an impurity centre (Fe^{3+}) due to iron present in a concentration smaller than 0.3 p.p.m. These measurements indicated the localization of the electron produced by the light irradiation of the semiconductor. For amorphous films, the electron is trapped in a defect ($g = 2.01 \pm 0.01$) or in an impurity centre ($g = 4.29 \pm 0.06$).

This is not the case for powders treated at 500 and 600 °C, whose electronic behaviour is very similar to that found in sodium metals [10]. There is a defect centre for the powder treated at 500 °C ($g = 2.02 \pm 0.03$) ; however, the signal is broad, indicating the presence of other contributions such as a NbO_6 unit in the semiconductor network [11]. According to Kim *et al.* [11], this defect centre is a hole mainly localized on an oxygen atom and near a niobium atom. In this way, the expected ten line for a Nb^{4+} centre with $g \cong 1.89$ [12] was not observed. There is no defect centre for the powder treated at 600 °C, suggesting the presence of a well-defined crystalline structure. At this temperature, electrons will be generated that are free to produce a photocurrent without recombination. This metallic behaviour is not present for the powder treated at 800 °C. The electrons are again trapped in a hole defect centre ($g = 2.03 \pm 0.04$). The electron generation is very small, indicating an insulating characteristic for the powder treated at this temperature.

3.3. Surface analysis of the films

The film surface was analysed by using a scanning electron microscope (SEM) and an energy dispersive spectrometer (EDS) where the changes introduced by the heat treatment in the morphology of the coating surface were observed at two different magnifications (Fig. 3). All the films were obtained from the same butoxide solution with only one deposition on an ITO substrate. Fig. 3a shows the coating surface for the treatment at 400 °C. The EDS identified niobium as being present in the white regions corresponding to the film of Nb_2O_5, and indium and tin of the substrate in the black regions. The EDS did not detect chlorine at the film surface. Note that the film is constituted of small particles whose diameter is smaller than 100 nm. Fig. 3b shows that the Nb_2O_5 particles undergo one sintering process which increases with temperature. This phenomenon is very clear in Fig. 3c.

3.4. Optical absorption of the films

The optical absorption measurement for coatings ($d = 40 \pm 4$ nm) is shown in Fig. 4. All the coatings

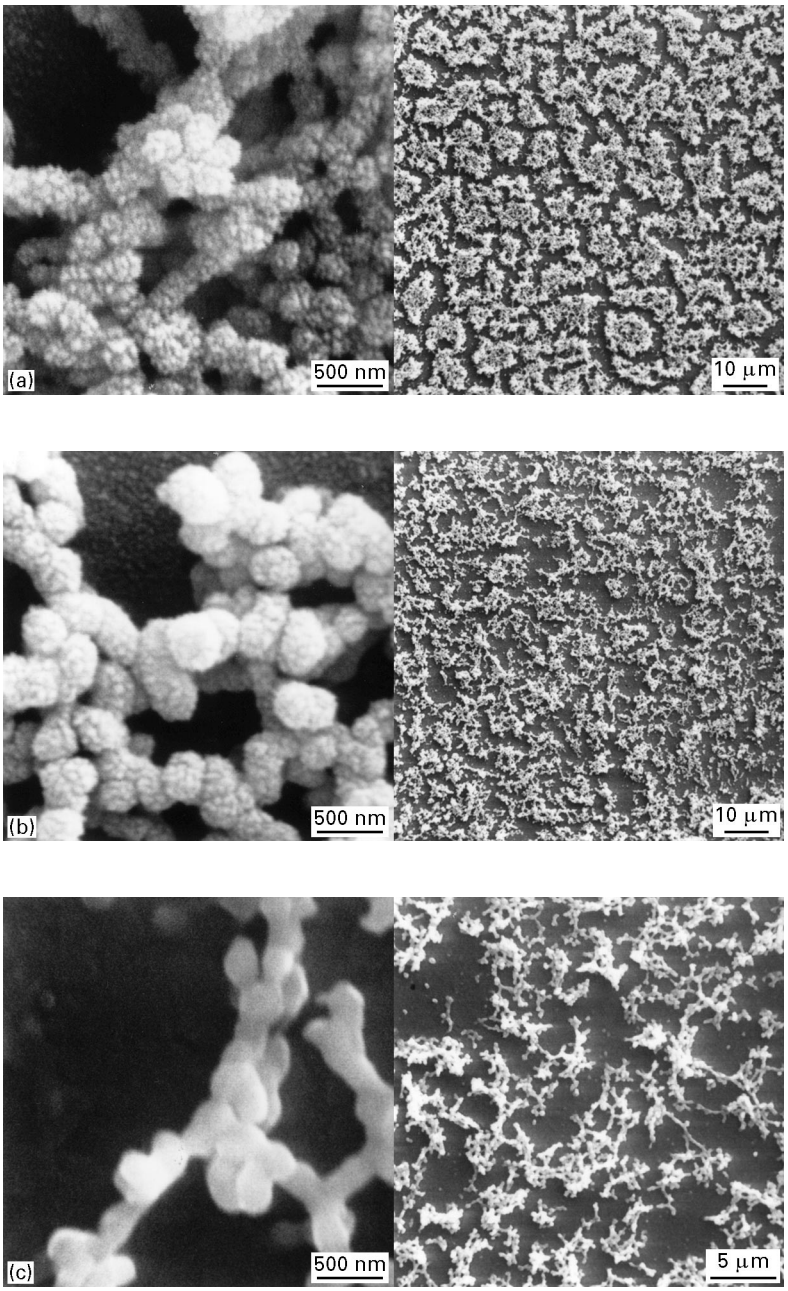

Figure 3 Electron micrograph of 100 nm films treated at different heat-treatment temperatures: (a) 400 °C (6.0% mol/mol); (b) 500 °C (3.0% mol/mol); (c) 600 °C (3.0% mol/mol).

showed an absorption band in the ultraviolet region associated with a charge-transfer process ($O^{2-} \rightarrow Nb^{5+}$). Also noted was a tail for $\lambda \geqslant 325$ nm which is associated with the presence of electrons in the mobility gap region and obeying the Urbach law [13].

The energy gap, E_g, for amorphous films was determinated by the Tauc and Demiryont [14, 15] relation

$$(\alpha h\nu)^{1/2} = A'(h\nu - E_g) \quad (1)$$

where A' is an experimental constant. Table I shows the E_g values obtained for the coatings. The largest dispersion of the E_g values was for the coating treated at 560 °C associated possibly with the coexistence of the $\delta \rightarrow \gamma$ phases for Nb_2O_5 [8]. Di Quartzo *et al.* [16] obtained optically $E_g = 3.35 \pm 0.05$ eV for amorphous anodic films of Nb_2O_5. This result agrees with the value found for the coating treated in this work at 400 °C.

The energy gap values have also been obtained photoelectrochemically for films whose thickness was 40 nm and heated at different temperatures (400, 500 and 600 °C). The gap value was determined using the relation

$$(ih\nu/I)^m = \mathbf{B}(h\nu - E_g) \quad (2)$$

where $m = 1/2$ corresponds to an indirect transition and $m = 2$ corresponds to a direct transition [17], i is the photoelectrochemical current, I is the light intensity, B is an experimental constant, v is the light frequency, h is the Planck constant, E_g is the gap energy. The results indicated an indirect transition and a value of $E_g = 3.39 \pm 0.05$ eV without significant variations with the heat-treatment temperature (Table I). These values are close to those obtained optically and agree with the photoelectrochemical determinations of Clechet *et al.* [18] for Nb_2O_5 coatings ($E_g = 3.4$ eV).

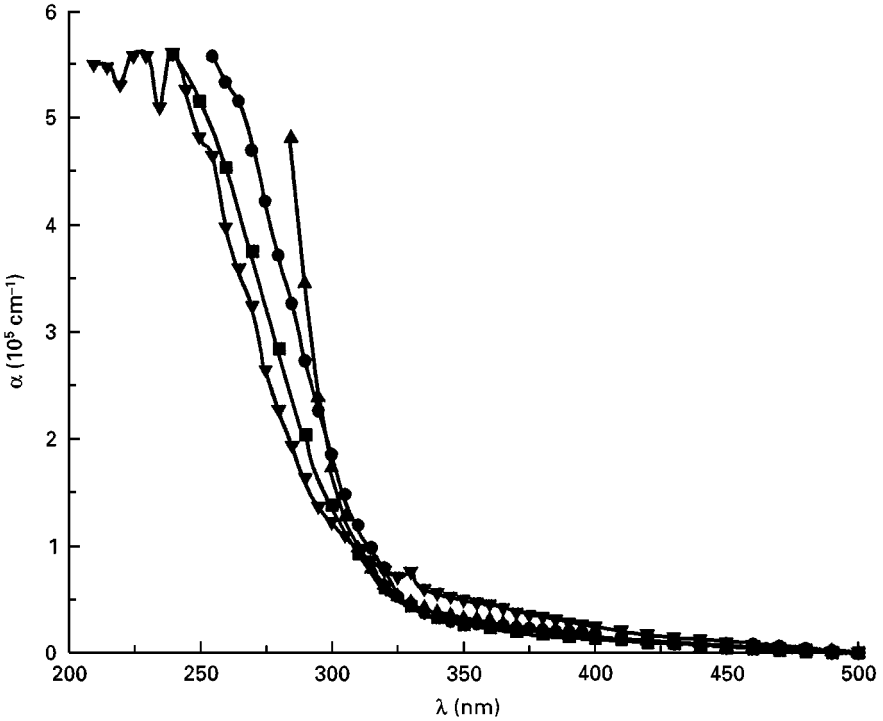

Figure 4 Absorption coefficient for Nb_2O_5 coatings treated at different heat-treatment temperatures: (■) 400 °C; (●) 500 °C; (▲) 560 °C; (▼) 600 °C. α is the absorption coefficient, λ the light wavelength.

TABLE I Energy gap values measured by optical absorption, E_{OG}, and by photoelectrochemical current, E_{EG}. T is the heat-treatment temperature

	T(°C)			
	400	500	560	600
E_{OG}(eV)	3.4 ± 0.2	3.5 ± 0.2	3.7 ± 0.7	3.5 ± 0.2
E_{EG}(eV)	3.37 ± 0.05	3.41 ± 0.03	–	3.39 ± 0.04

3.5. Photoelectrochemical behaviour for films

Polarization curves were obtained in order to verify the chemical reactions occurring at the SEI. In this way, experiments with different wavelengths (250–400 nm) were realized in electrolytical solutions saturated with nitrogen or oxygen. The polarization curves shown in Fig. 5a were obtained with a constant wavelength (λ = 320 nm) and different intensities of light (0–100%). It was possible to determine the charge-transfer coefficient, α_e, described by the Butler–Volmer equation [19] from the results presented in Fig. 5a. The α_e value determined was 0.935 ± 0.003, which is typical for an n-type semiconductor. Fig. 5b shows the variation of the photocurrent with the light intensity for a constant potential ($E = +0.4$ V). It was observed that the photoelectrochemical current increases with the light transmission percentage (Fig. 5b). The linear fit indicates that, under the experimental conditions used, the electrochemical reactions of water electrolysis did not limit the photoelectrochemical process [20]. This procedure was also used to verify the

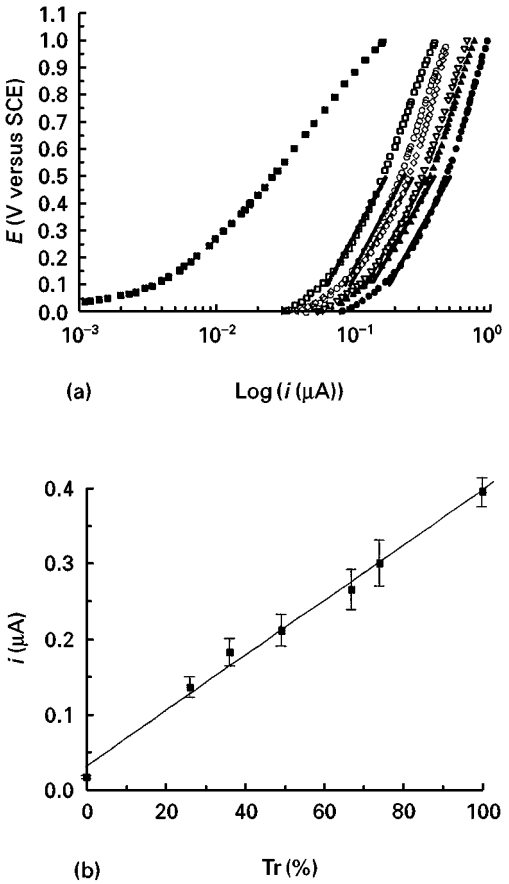

Figure 5 Photoelectrochemical behaviour for Nb_2O_5 coating in an aqueous medium ($d \approx 240$ nm) treated at 560 °C/2 h with varying light intensity (λ = 320 nm): (a) polarization curve ($v = 1$ mV s^{-1}); (b) current for fixed potential ($E = +0.4$ V). i is the photoelectrochemical current, E the applied potential, Tr the transmitted light ratio, v the scan velocity, λ the light wavelength, d the film thickness. (a) Tr: (■) 0%, (□) 26%, (○) 36%, (◇) 49%, (▽) 67%, (▲) 74%, (●) 100%.

stability of the film during the photoelectrochemical measurement. It was observed that the photocurrent was not zero for the transmittance equal to 0% because of the existence of very low electrochemical currents without light irradiation ($i = 17.7$ nA).

Fig. 6a shows the polarization curves relative to the variation of the wavelength in a nitrogen-saturated electrolyte. The results showed that there is an increase of the current with the applied potential, indicating the presence of water electrolysis. The flat-band potential was determined by the plot of i^2 versus λ and the value found was equal to $V_{bp} = 0.11$ V.

Fig. 6b shows the polarization curve ($v = 1\ \mathrm{mV\,s^{-1}}$) relative to the variation of the wavelength in the oxygen-saturated electrolyte. The current is about 50% smaller than that obtained with the nitrogen-saturated electrolyte (Fig. 6a) because the oxygen acts as an electron collector in the SEI, decreasing the current value. Hagfeldt *et al.* [21] argued that oxygen can play an important role in the recombination process of the electrons due to the increase of the hole concentration along the semiconductor surface. The anomalous behaviour of the current for $\lambda \leqslant 280$ nm is different from $\lambda \geqslant 300$ nm because the generation of holes close to the semiconductor surface increases for low wavelengths. The flat-band potential was determined by the plot of i^2 versus λ and its value corresponded to $V_{bp} = 0.11$ V.

The measurement of the normalized action spectra was made by changing the following parameters: heat treatment, coating thickness and solvent for the electrolyte. Fig. 7a shows the quantum yield in aqueous $LiClO_4$ electrolyte ($0.2\ \mathrm{mol\,l^{-1}}$) for three films (thickness 40 nm) prepared with different heat treatments (400, 500 and 600 °C). The photocurrents were measured without applied potential ($E = 0.0$ V) . Note that the best performance was obtained for the film treated at 600° C but the quantum yield, ϕ, was still low when compared with TiO_2 colloidal coatings [22]. Fig. 7b shows the quantum yield for films with different thicknesses. In this case, two aspects were observed due to the increase of the film thickness: the maximum shift into longer wavelengths and a significant decrease of the quantum yield.

The action spectra for the films (Fig. 8c) using a $LiClO_4$ solution $1\ \mathrm{mol\,l^{-1}}$ in propylene carbonate were obtained from measurements of light power and current versus wavelength (Fig. 8a and b). The films were prepared using a solution of niobium chlorobutoxide (1.5% mol/mol) and were densified at different temperatures (400, 500 and 600 °C). The film surface was shown to be rugged with a thickness

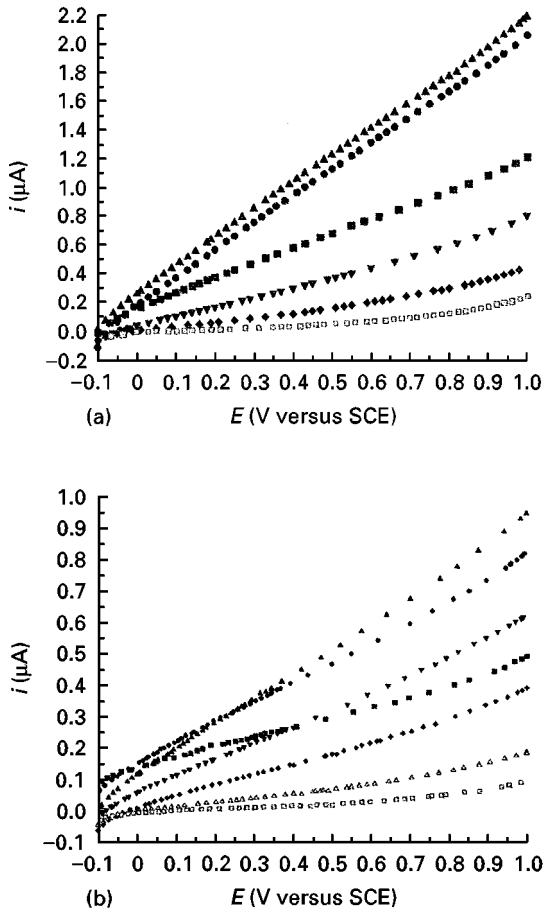

Figure 6 Polarization curves ($v = 1\ \mathrm{mV\,s^{-1}}$) for Nb_2O_5 coating in an aqueous medium ($T = 560$ °C/2 h and $d \approx 240$ nm) subjected to different wavelengths: (a) nitrogen saturation; (b) oxygen saturation. i is the photoelectrochemical current, λ the light wavelength, d the film thickness, E the applied potential, v the scan velocity. T the heat treatment temperature. λ: (a) (■) 250 nm, (●) 275 nm, (▲) 300 nm, (▼) 330 nm, (◆) 350 nm, (□) 400 nm; (b) (■) 250 nm, (●) 275 nm, (▲) 300 nm, (▼) 315 nm, (◆) 330 nm, (△) 350 nm, (□) 375 nm.

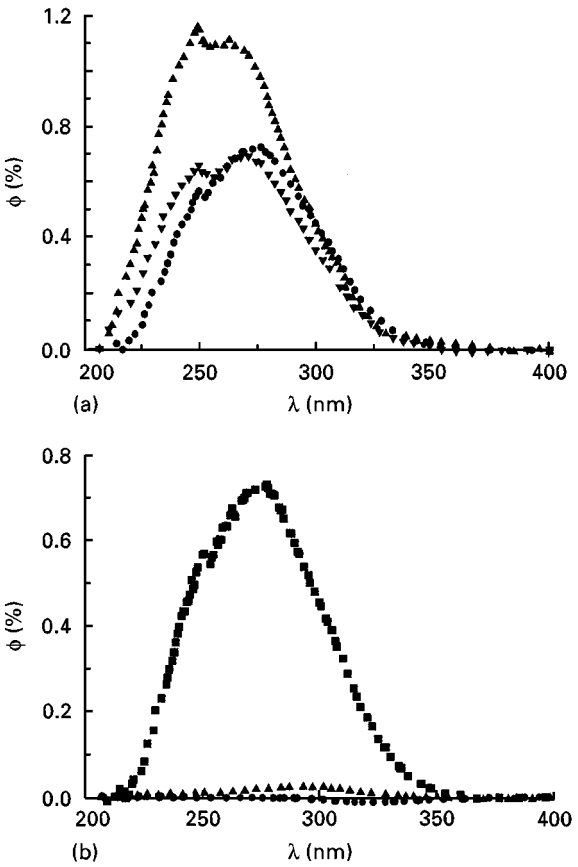

Figure 7 Quantum yield behaviour for Nb_2O_5 films in an aqueous medium: (a) different heat-treatment temperatures, (▼) 400 °C/2 h, (●) 500 °C/2 h, (▲) 600 °C/2 h; (b) thickness variation ($T = 500$ °C/2 h), (■) 40 nm, (▲) 120 nm, (●) 240 nm. ϕ is the quantum yield for electrolyte-electrode illumination, λ the wavelength, d the film thickness.

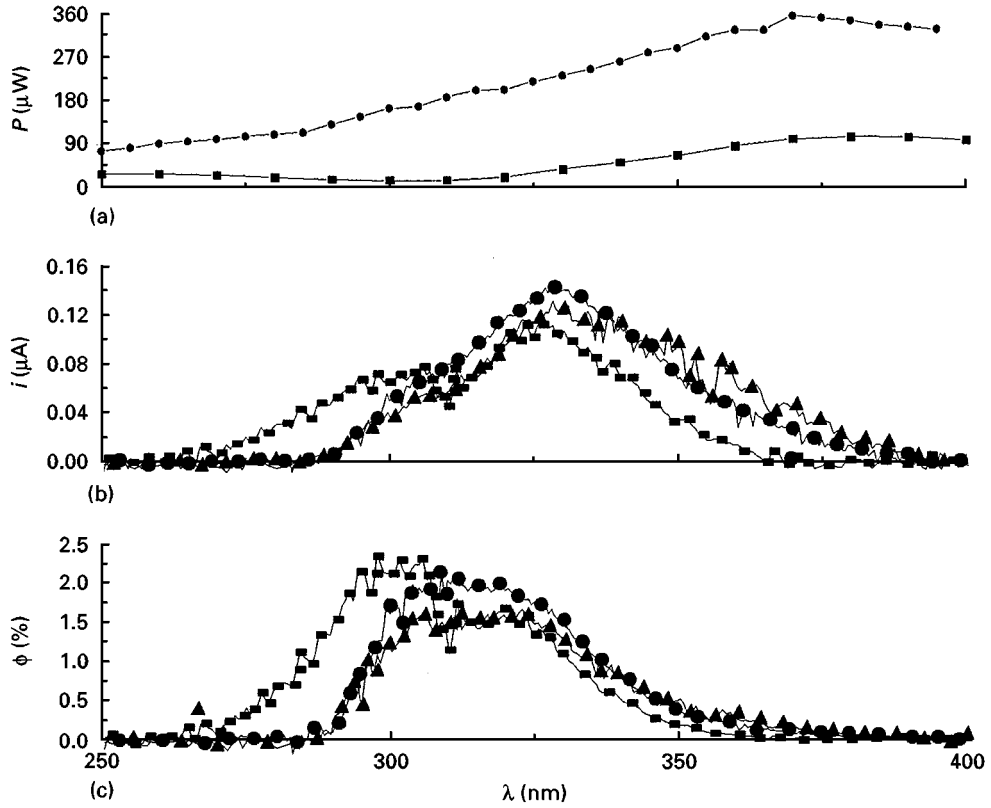

Figure 8 Photoeletrochemical behaviour of Nb_2O_5 coatings treated at different temperatures in propylene carbonate ($C = 1$ M): (a) light power at the film surface in (■) water, and (●) propylene carbonate; (b) photoelectrochemical current; (c) quantum yield. λ is the light wavelength, C the molar concentration, P the light power, ϕ the quantum yield for electrolyte-electrode illumination, T the heat treatment temperature, i the photoelectrochemical current. (b, c) T: (■) 400 °C, (●) 500 °C, (▲) 600 °C.

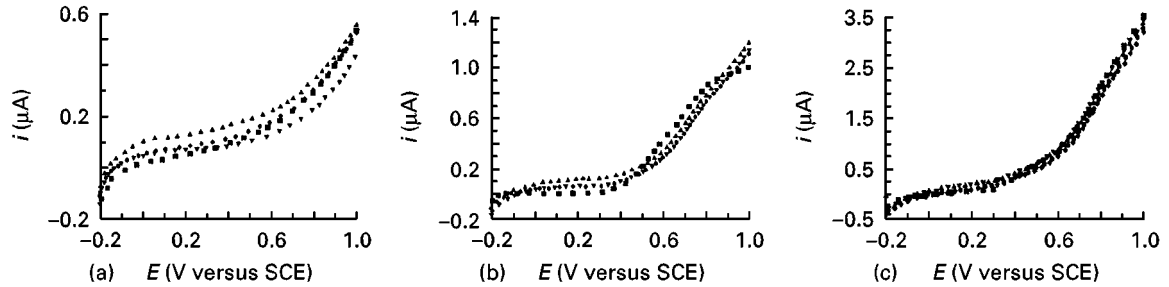

Figure 9 Polarization curves ($v = 1\,\mathrm{mV\,s^{-1}}$) for Nb_2O_5 coatings in propylene carbonate ($C = 1$ M): (a) $T = 400$ °C; (b) $T = 500$ °C; (c) $T = 600$ °C. i is the photoelectrochemical current, λ the light wavelength, E the applied potential, v the scan velocity, C the molar concentration. λ: (■) 280 nm, (●) 300 nm, (▲) 330 nm, (▼) 350 nm, (◆) 370 nm.

around 100 ± 20 nm. Fig. 8a shows the power of light incident on the film surface using water and propylene carbonate as solvent. Note that there is a minimum around 300 nm for propylene carbonate that influences the photoelectrochemical behaviour in this region increasing the quantum yield for the film treated at 400 °C (Fig. 8c). The photoelectrochemical behaviour is practically the same for the films treated at 500 and 600 °C (Fig. 8b). The maximum quantum yield observed for the film treated at 400 °C is only a consequence of the fact that a minimum is present in the light power at this wavelength as shown in Fig. 8a. The quantum yield increases by approximately twice in comparison with that shown in Fig. 7a. This fact is possibly associated with the utilization of propylene carbonate as solvent.

Polarization curves for different wavelengths were obtained for the same films shown in Fig. 8 with propylene carbonate (Fig. 9). The results indicated that there is a plateau in the range $0.0 \leqslant E \leqslant 0.2$ V. This did not happen in an aqueous electrolyte, indicating an electrochemical stability during the measurement. Note that the photocurrent for the film treated at 600 °C is bigger than that measured for other films.

The normalized spectra were analysed by the Södergren model [23] in order to determine the diffusion length of the electron in the semiconductor. The thickness values for the coatings have already been

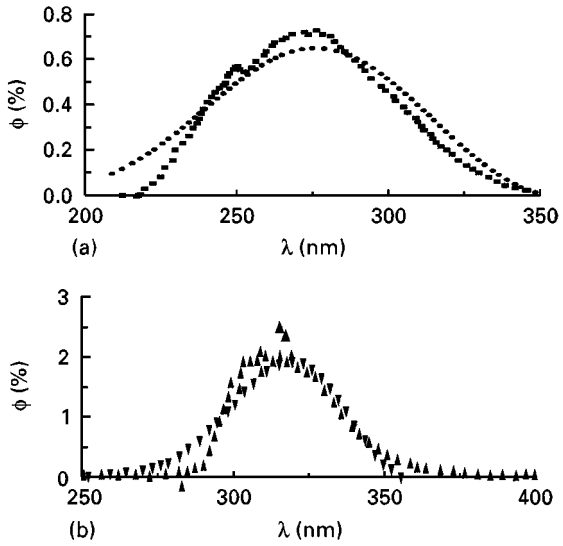

Figure 10 Södergren model for Nb_2O_5 coatings with different thicknesses and treated at 500 °C: (a) $d = 40$ nm (water); (b) $d = 100$ nm (propylene carbonate). ϕ is the quantum yield for electrolyte-electrode illumination, λ the wavelength of light, d the film thickness. ϕ: (■, ▲) measured; (●, ▼) calculated.

determined by profilometry. According to Södergren, the quantum yield, ϕ, for nanocrystalline porous films is given by

$$\phi = \left[L\alpha\cosh\left(\frac{d}{L}\right) + \sinh\left(\frac{d}{L}\right) - L\alpha e^{\alpha d}\right]L\alpha e^{-\alpha d} \Bigg/ \left\{\left[1-(\alpha L)^2\right]\cosh\left(\frac{d}{L}\right)\right\}. \quad (3)$$

where d is the film thickness, α is the optical absorption coefficient of the film, and L is the electron diffusion length.

Fig. 10a shows the fit according to the Södergren model for a film treated at 500 °C and with thickness of 40 ± 4 nm. The solvent used was water. The values obtained by the fit were $L = 0.43 \pm 0.01$ nm and $d = 24.8 \pm 0.4$ nm. Note that the calculated thickness value does not agree with that measured by profilometry. Fig. 10b shows the fit for the film whose thickness was estimated to be around 100 nm and treated at 500 °C. The solvent used was propylene carbonate. The fitting resulted in $L = 6.5 \pm 0.2$ nm and $d = 129 \pm 2$ nm. Note that this is closer to the thickness measured by profilometry. The adjusted fit was good for both films with $\chi^2 \leqslant 10^{-6}$ for a tolerance corresponding to 0.05.

4. Discussion

The Nb_2O_5 is an oxide semiconductor whose properties are similar to TiO_2: energy gap ($E_g = 3.03$ eV) [17], indirect transition and electronic structure. The sol–gel process is used in order to produce Nb_2O_5 gels [24] and coatings [25]. This semiconductor has an accentuated polymorphism [26] and a great variety in its surface morphology [27]. The X-ray measurements (Fig. 1) indicated that the crystalline structure of the semiconductor is significantly changed in the region 500 °C < T < 1000 °C. According to Terao [8], two factors influence the semiconductor crystalline structure: oxygen content in air and the heating time.

The photoelectrochemical properties of Nb_2O_5 coatings have been described in some works [16, 28]. However, the electronic transition involved in this process is still not well understood. The EPR measurements indicated that there is not a reduction reaction ($Nb^{5+} \rightarrow Nb^{4+}$) with a typical ten line spectrum (Fig. 2) [11]. The electron is trapped in a hole defect centre associated with oxygen atoms. The most important result of the EPR measurements is the metallic behaviour observed for powders treated at 500 and 600 °C. There are significant changes in the optical and photoelectrochemical behaviour in this temperature range (Figs 4, 7a and 7b). It is possible that this metallic behaviour can be explained by the presence of an intermediate phase $\delta(\gamma)$ or $\gamma(\delta)$ described by Terao [8].

Nowadays, there are two principal models for the charge transport at SEI: those of Gärtner [29] and Södergren [23]. The quantum yield of electrolyte–electrode illumination, ϕ_{EE}, and the quantum yield of substrate–electrode illumination, ϕ_{SE}, are just the opposite, according to the two models (Fig. 11). The Gärtner model considers the SEI to be like a Schottky barrier, where the electric field inside the semiconductor causes the charge separation (Fig. 11a). According to Curran and Lamouche [30], the electric field for colloidal particles would be close to 50 mV. However, measurements done by O'Regan *et al.* [31] indicated that the maximum potential difference between the centre and the surface of colloidal particles would be 0.3 mV. For this reason, there can be no flat-band potential for the semiconductor nanocrystalline coatings (TiO_2 and Nb_2O_5).

The Södergren model considers the nanocrystalline semiconductor film to consist of colloidal particles (Fig. 11b). In this way, the electrolyte diffusion occurs along the whole film extension and, consequently, there is no electric field inside the semiconductor. The absence of an electric field means the charge transport for nanocrystalline films is a diffusional process. The electric current is formed mainly by electrons whose generation occurs at a distance L in the conductor film. This distance corresponds to the electron diffusion length in the semiconductor.

The photoelectrochemical measurements in this work indicated that the charge transfer at SEI obeys the Södergren model. However, the L values for Nb_2O_5 coatings are very small when compared to those obtained for TiO_2 coatings by Södergren ($L = 800$ nm and $d = 2.500$ nm). This parameter is an intrinsic property of the semiconductor, but it can be changed with adequate film preparation. This fact was observed in the photoelectrochemical measurements, where the L value for a film with a thickness of 100 nm was approximately ten times higher than 40 nm. This fact is due to surface morphology and type of solvent. The surface morphology allowed a better diffusion of the electrolyte with a most effective charge separation in the film constituted by an agglomeration of particles smaller than 100 nm (Fig. 3). Another aspect is the utilization of propylene carbonate which does not

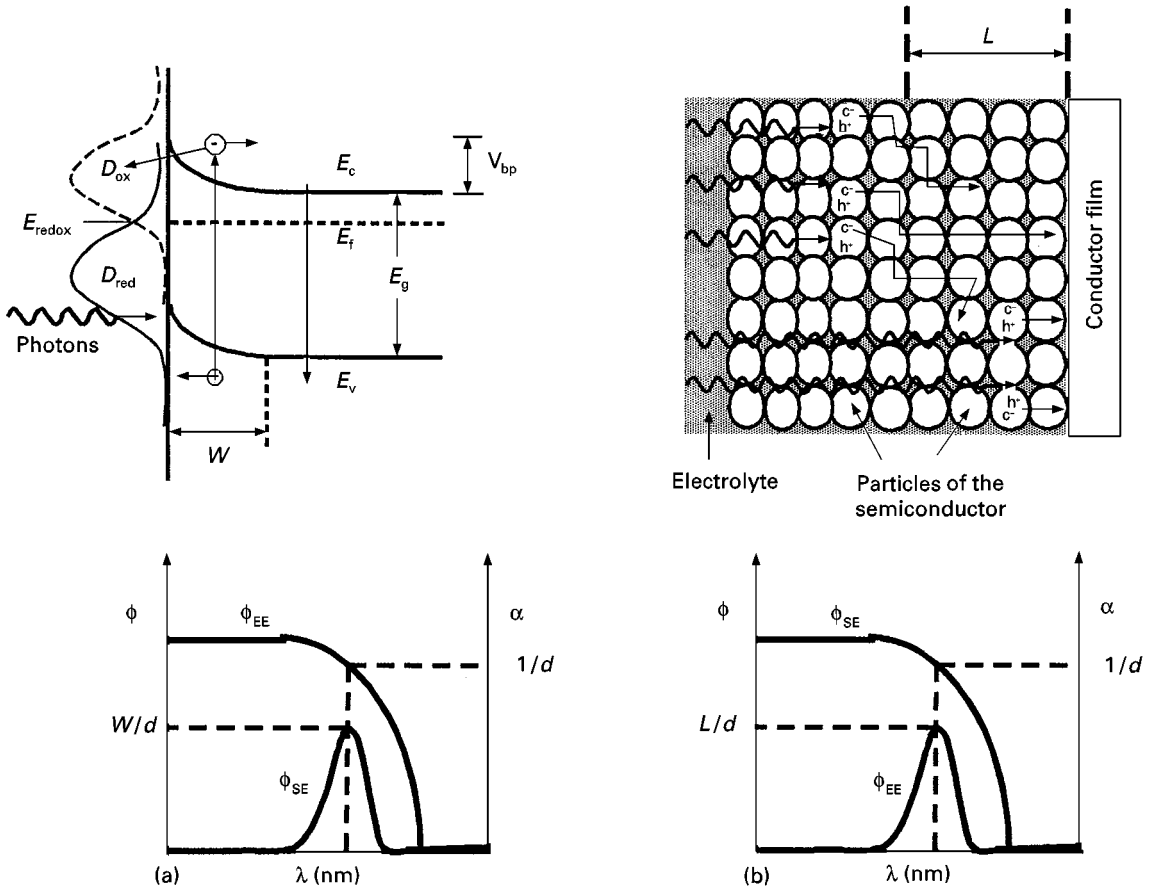

Figure 11 The charge transfer model: (a) Gärtner–Schottky (solid films); (b) Södergren (colloidal films). L is the electron diffusion length, V_{bp} the flat-band potential, E_c the bottom energy level of the conduction band, E_v the top energy level of the valence band, E_g the gap energy, E_f the Fermi energy, W the depletion length, E_{red} the redox energy, D_{ox} the energy distribution for oxidized molecules, D_{red} the energy distribution for reduced molecules, ϕ the quantum yield, ϕ_{EE} the quantum yield for electrolyte–electrode illumination, ϕ_{SE} the quantum yield for substrate–electrode illumination, λ the light wavelength, α the optical absorption coefficient, e^- the photogenerated electron, h^+ the photogenerated hole, d the film thickness.

undergo decomposition reactions on the semiconductor surface (Fig. 9). These two factors are responsible for the increase in the quantum yield in this thicker film.

Another aspect was the differences between the thickness measured by profilometry and that calculated by the Södergren model. The effective region in these films for charge transfer is not the film thickness, as was proposed by the Södergren model. The thickness value calculated for 40 nm films corresponded to the diffusion length of the electrolyte inside the semiconductor structure. It was different for the 100 nm film, where the electrolyte diffusion and the film thickness values are approximately the same.

The surface for the 100 nm film is irregular and its thickness value can be considered to be in the range 100–200 nm. This variation was not significant for fitting with the Södergren model. The maximum shift indicated that the electrolyte was able to penetrate inside the film. The higher quantum yield for 100 nm films is a consequence mainly of the film surface that prevents recombination, and the non-aqueous electrolyte that allows a better ion diffusion along the semiconductor. A higher quantum yield was expected for 100 nm films with a maximum corresponding to $\phi = L/d \cong 6\%$. However, there were losses that cannot be disregarded, such as recombination processes, surface states and so on.

The application of Nb_2O_5 coatings is possible in photovoltaic dispositives with the incorporation of polypyridine complexes, shifting the spectra to the visible region. In this case, the quantum yield obtained may be higher because the charge transfer would not involve the formation of holes inside the semiconductor film. The utilization of an electrolyte with a redox couple may also improve the quantum yield for values close to TiO_2.

5. Conclusion

The process of photocurrent generation for Nb_2O_5 coatings was discussed in terms of their structural, electronic and optical properties. The quantum yield for these coatings was analysed in terms of their surface morphology and heat treatment. A high quantum yield was observed for coatings treated close to 600 °C, associated with modifications in the crystalline structure of the semiconductor. The charge transfer process obeys the Södergren model where the porosity of the surface plays an important role.

Acknowledgements

This research was sponsored by Conselho Nacional de Desenvolvimento Cientifico e Tecnológico (CNPq),

Fundacão de Amparo à Pesquisa do Estado de São Paulo (FAPESP) and Financiadora dc Estudos e Projetos (FINEP). The niobium pentachloride was supplied by Companhia Brasileira de Metalurgia e Mineracão (CBMM). The first steps of this work were followed by Dr M. A. Aegerter, and an important contribution was made by Dr B. R. McGarvey. The EPR measurements were performed by Dr Luis Constantino de Vasconcelos. The help of Marcos José Semenzato Geraldo Mangerona Frigo and Manoel Ricardo Pereira on the photoelectrochemical cell experiments is also gratefully acknowledged. The photoelectrochemical measurements were performed at Instituto de Fisica de São Carlos (IFSC).

References

1. M. GRÄTZEL, *Coord. Chem. Rev.* **111** (1991) 167.
2. *Idem.*, *Comments Inorg. Chem.* **12** (1991) 93.
3. *Idem.*, *MRS Bull.* **XVIII** (1993) 61.
4. C. A. KOVAL and J. N. HOWARD, *Chem. Rev.* **92** (1992) 411.
5. M. K. NAZEERUDDIN, A. KAY, I. RODICIO, R. HUMPHRY-BAKER, E. MÜLLER, P. LISKA, N. VLACHOPOULOS and M. GRÄTZEL, *J. Am. Chem. Soc.* **115** (1993) 6382.
6. D. C. BRADLEY, B. N. CHAKRAVARTI and W. WARDLAW, *J. Chem. Soc.* (1956) 2381.
7. J. BASSET, R. C. DENNEY, G. H. JAFFERY, J. MENDHAM, in "Vogel-análise Inorganica Quantitativa", 4th Edition, (Guanabara Dois, Rio de Janeiro, 1981) p. 253.
8. N. TERAO, *Jpn. J. Appl. Phys.* **2** (1963) 156.
9. D. L. GRISCOM, in "Glass: Science and Technology", edited by D. R. Uhlmann and N. J. Kreidl (Harcourt Brace Jovanonovich, Arizona, 1990) p. 151.
10. F. VESCIAL, N. S. VANDERVEN and R. T. SCHUMACHER, *Phys. Rev.* **134** (1964) A1286.
11. Y. M. KIM, D. E. REARDON and P. J. BRAY, *J. Chem. Phys.* **48** (1968) 3396.
12. M. SUGANTHA and G. V. SUBBA RAO, *J. Solid State Chem.* **111** (1994) 33.
13. F. URBACH, *Phys. Rev.* **92** (1953) 1324.
14. J. TAUC, in "Amorphous and Liquid Semiconductors", (Plenum, New York, 1974).
15. H. DEMIRYONT, J. R. SITES and K. GEIB, *Appl. Optics* **24** (1985) 490.
16. F. Di QUARTZO, S. PIAZZA, R. D'AGOSTINO and C. SUNSERI, *J. Electroanalyt. Chem.* **228** (1987) 119.
17. T. YOKO, A. YAUSA, K. KAMIYA and S. SAKKA, *J. Electrochem. Soc.* **138** (1991) 2279.
18. P. CLECHET, J. R. MARTIN, R. OLIER and C. VALLOUY, *C.R. Acad. Sci. Paris* **282** (1976) 887.
19. J. O. M. BOCKRIS and A. K. N. REDDY, in "Modern Electrochemistry" Vol. **2** (Plenum/ Rosetta, New York, 1970) p. 862.
20. M. A. BUTLER, *J. Appl. Phys.* **48** (1977) 1914.
21. A. HAGFELDT, H. LINDSTRÖM, S. SÖDERGREN and S.-E. LINDQUIST, *J. Electroanalyt. Chem.* **381** (1995) 39.
22. A. HAGFELDT,U. BJÖRKSTÉN and S. E. LINDQUIST, *Solar Energy Mater. Solar Cells* **27** (1992) 293.
23. S. SÖDERGREN, A. HAGFELDT, J. OLSSON and S. E. LINDQUIST, *J. Phys. Chem.* **98** (1994) 5552.
24. P. GRIESMAR, G. PAPIN, C. SANCHEZ and J. LIVAGE, *Chem. Mater.* **3** (1991) 335.
25. N. ÖZER, T. BARRETO, T. BÜYÜKLIMANLI and C. M. LAMPERT, *Solar Energy Mater. Solar Cells* **36** (1995) 433.
26. H. SCHÄFER, R. GRUEHN and F. SCHULTE, *Angew. Chem. Int. Ed.* **5** (1966) 40.
27. L. HU, W. MARCUS, M. GRÄTZEL and Z. JIANG, *J. Sol Gel Sci. Technol.* **5** (1995) 219.
28. M. ARITA and Y. HAYASHI, *Mater. Trans. JIM* **35** (1994) 233.
29. W. W. GÄRTNER, *Phys. Rev.* **116** (1959) 84.
30. J. S. CURRAN and D. LAMOUCHE, *J. Phys. Chem.* **87** (1983) 5405.
31. B. O'REGAN, J. MOSER, M. ANDERSON and M. GRÄTZEL, *J. Phys. Chem.* **94** (1990) 8720.

Received 24 February 1997
and accepted 27 January 1998